PAPER

Self-organization in dc glow microdischarges in krypton: modelling and experiments

To cite this article: W Zhu *et al* 2014 *Plasma Sources Sci. Technol.* **23** 054012

IOP Publishing Plasma Sources Science and Technology

Plasma Sources Sci. Technol. **23** (2014) 054012 (6pp) doi:10.1088/0963-0252/23/5/054012

Self-organization in dc glow microdischarges in krypton: modelling and experiments

W Zhu[1], P Niraula[1], P G C Almeida[2], M S Benilov[2,3] and D F N Santos[2]

[1] Department of Applied Science, Technology, Saint Peter's University, 2641 Kennedy Boulevard, Jersey City, NJ 07306, USA
[2] CCCEE, Universidade da Madeira, Largo do Município, 9000 Funchal and Portugal

E-mail: benilov@uma.pt

Received 22 January 2014, revised 15 May 2014
Accepted for publication 10 June 2014
Published 25 September 2014

Abstract

Self-organized patterns of cathodic spots have been observed in microdischarges operated in xenon, but not in other gases. However, modelling has indicated that it is, in principle, possible to observe the patterns of spots in discharges operated in other gases provided that experimental conditions, in particular pressure, are right. In this work, self-organized patterns of cathodic spots are for the first time observed in dc glow microdischarges operated in a gas other than xenon: krypton. The experiments have been guided by the modelling. According to both the experiment and the modelling, patterns in krypton are similar to those found earlier in xenon, however occur at higher pressures.

Keywords: glow discharges, self-organization, multiple solutions, bifurcations

(Some figures may appear in colour only in the online journal)

1. Introduction

Self-organized patterns of cathodic spots have been observed at the transition between the abnormal discharge and the normal discharge [1–7] and represent a highly interesting phenomenon. The patterns have been observed in microdischarges in xenon under the gas pressures from 75 to 760 Torr, but not in other gases such as argon [2, 3, 8] or krypton [3].

It has been shown recently [9–14] that there is no necessity in introducing new physical mechanisms in order to explain these observations: a new class of solutions has been found in the classical theory of glow discharges that dates back to the 1930s, and these solutions describe spot patterns similar to those observed in the experiment. According to the theory, self-organization in dc glow discharges is a general phenomenon and not particular of xenon. Although conditions of xenon microdischarges are indeed more favourable for the appearance of self-organization than microdischarges in, e.g. argon or helium, it has been shown [12–14] that multiple solutions exist in gases other than xenon provided that experimental conditions are right, in particular that the pressure is high enough. However, the experimental verification of this prediction has been lacking.

In this work, self-organization in microdischarges in gases other than xenon is reported for the first time. The experiments have been performed on glow microdischarges in krypton and were guided by the modelling. The outline of the paper is as follows. In section 2, the numerical model is briefly discussed and modelling results are given. In section 3, the experimental setup is described and experimental results on self-organization in microdischarges in krypton are given. Finally, conclusions are summarized in section 4.

2. Modelling

The aim of the modelling is to qualitatively describe self-organization in dc glow discharges in krypton in order to provide a guide for the experiment, rather than to achieve quantitative agreement with experimental results. Therefore, the most basic self-consistent model of dc glow discharge was employed. The model comprises equations of conservation of a single ion species and the electrons, transport equations

[3] Author to whom any correspondence should be addressed.

for the ions and the electrons written in the drift–diffusion approximation, and the Poisson equation:

$$\nabla \cdot \boldsymbol{J}_\mathrm{i} = n_\mathrm{e}\,\alpha\,\mu_\mathrm{e}\,E - \beta\,n_\mathrm{e}\,n_\mathrm{i}, \quad \boldsymbol{J}_\mathrm{i} = -D_\mathrm{i}\,\nabla n_\mathrm{i} - n_\mathrm{i}\,\mu_\mathrm{i}\,\nabla\varphi, \tag{1}$$

$$\nabla \cdot \boldsymbol{J}_\mathrm{e} = n_\mathrm{e}\,\alpha\,\mu_\mathrm{e}\,E - \beta\,n_\mathrm{e}\,n_\mathrm{i}, \quad \boldsymbol{J}_\mathrm{e} = -D_\mathrm{e}\,\nabla n_\mathrm{e} + n_\mathrm{e}\,\mu_\mathrm{e}\,\nabla\varphi, \tag{2}$$

$$\varepsilon_0\,\nabla^2\varphi = -e\,(n_\mathrm{i} - n_\mathrm{e})\,. \tag{3}$$

Here n_i, n_e, $\boldsymbol{J}_\mathrm{i}$, $\boldsymbol{J}_\mathrm{e}$, D_i, D_e, μ_i, and μ_e are number densities, densities of transport fluxes, diffusion coefficients, and mobilities of the ions and electrons, respectively; α is Townsend's ionization coefficient; β is coefficient of dissociative recombination; φ is electrostatic potential, $E = |\nabla\varphi|$ is electric field strength; ε_0 is permittivity of free space; and e is elementary charge.

Boundary conditions at the cathode and anode are written in the conventional form: diffusion fluxes of the attracted particles are neglected as compared to drift; the normal flux of the electrons emitted by the cathode is related to the flux of incident ions in terms of the effective secondary emission coefficient γ, which is assumed to characterize all mechanisms of electron emission (due to ion, photon and excited atom bombardment) [19]; density of ions vanishes at the anode; electrostatic potentials of both electrodes are given; zero electric current density normal to the wall of the discharge vessel, which is assumed to reflect impinging charged particles back to the discharge. Let us consider a discharge vessel in the form of a right circular cylinder of a radius R and of a height h, and introduce cylindrical coordinates (r, ϕ, z) with the origin at the centre of the cathode and the z-axis coinciding with the axis of the vessel. Then the boundary conditions read

$$z = 0: \ \frac{\partial n_\mathrm{i}}{\partial z} = 0, \quad J_{\mathrm{e}z} = -\gamma J_{\mathrm{i}z}, \quad \varphi = 0; \tag{4}$$

$$z = h: \ n_\mathrm{i} = 0, \quad \frac{\partial n_\mathrm{e}}{\partial z} = 0, \quad \varphi = U; \tag{5}$$

$$r = R: \ \frac{\partial n_\mathrm{i}}{\partial r} = \frac{\partial n_\mathrm{e}}{\partial r} = 0, \quad J_{\mathrm{i}r} - J_{\mathrm{e}r} = 0. \tag{6}$$

Here U is the discharge voltage, the subscripts r and z denote radial and axial projections of corresponding vectors.

It should be stressed that this simple model is adequate for a qualitative investigation of multiple solutions; the inclusion in the model of a more detailed kinetic scheme and non-locality of electron transport and kinetic coefficients does not significantly affect their pattern [14]. A detailed description of the procedure of finding multiple solutions can be found in [16].

Modelling is performed for krypton; some results for xenon are also shown for comparison. 1D modelling is performed for an interelectrode gap h of 250 μm; 3D modelling is performed for a cylindrical discharge vessel with $h = 0.5$ mm and radius R of 0.5 mm. The (only) ionic species considered in the modelling is Kr_2^+. The mobility of Kr_2^+ ions in Kr was evaluated by means of the formula $\mu_\mathrm{i} = 3.3 \times 10^{21}\ \mathrm{m^{-1}V^{-1}s^{-1}}/n_n$ (here n_n is the density of the neutral gas) [18]. The mobility of the electrons is evaluated as $\mu_\mathrm{e} = 13\ \mathrm{Torr\,m^2V^{-1}s^{-1}}/p$ (here p is the neutral gas pressure).

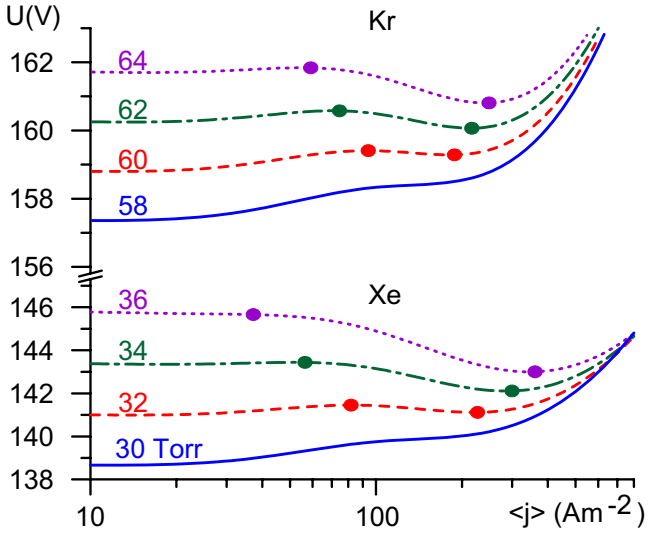

Figure 1. CDVC of the 1D mode, $h = 250\,\mu$m, $R = 375\,\mu$m. Lines: CDVC for different pressures. Circles: bifurcation points where the first 3D mode branches off from or rejoins the 1D mode.

Townsend's ionization coefficient was evaluated by means of the formula [19] $\alpha = Cp\exp[-D(p/E)^{1/2}]$ with $C = 3.57\times10^3\ \mathrm{m^{-1}Torr^{-1}}$ and $D = 2.82\times10^2\ \mathrm{V^{1/2}m^{-1/2}Torr^{-1/2}}$. (It has been verified that these formulas yield results for μ_e and α which are in good agreement with those given by the zero-dimensional Boltzmann solver BOLSIG+ [20].) The diffusion coefficients were evaluated by means of Einstein's law with $T_\mathrm{i} = 300$ K and $T_\mathrm{e} = 1$ eV. The coefficient of dissociative recombination of molecular ion was set equal to $9.8 \times 10^{-12}\ \mathrm{m^3s^{-1}}$ [21]. The effective secondary electron emission coefficient was set equal to 0.03. The data used in the modelling for xenon can be found in [10].

Previous experiments for xenon [4] have shown that the self-organized patterns observed in microdischarges in the above-described cathode boundary layer discharge (CBLD) electrode configuration are similar to those observed in discharges with parallel-plane electrodes. For this reason, the modelling was performed for a cylindrical discharge vessel with parallel-plane electrodes. Results reported in this work refer to the case of a reflecting lateral wall, see boundary condition for electrons and ions in equation (6); in other words, neutralization of charged particles at the wall is neglected. This assumption significantly reduces the computation time; the effect of neutralization of charged particles at the wall over multiple solutions may be studied at a later stage similarly to how it was done in [14].

Figure 1 depicts the current density–voltage characteristics (CDVC) of the 1D mode, i.e. the mode in which discharge parameters vary in the axial direction only, computed for different pressures in krypton and xenon. Also shown are the bifurcation points where the first 3D mode branches off from or rejoins the 1D mode. (These points were computed for the discharge tube radius of 0.375 mm by means of bifurcation analysis of the 1D mode using the method described in [9].) For $p = 64$ Torr for krypton and $p = 36$ Torr for xenon, one of the two bifurcation points is positioned at the beginning of the falling section of CDVC, while the other is positioned close

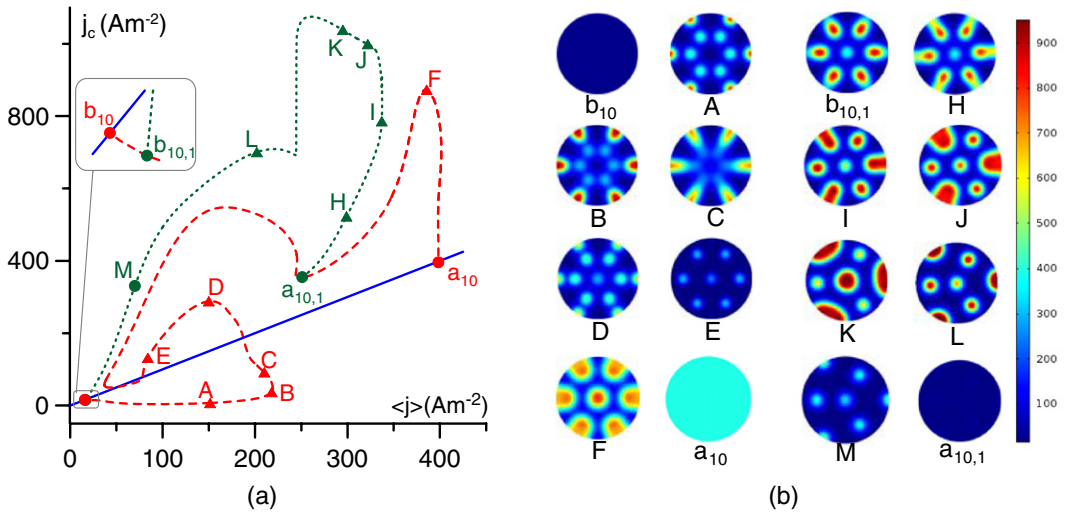

Figure 2. (*a*) Bifurcation diagram of 3D modes in krypton, $R = h = 0.5$ mm. Solid line: 1D mode. Dashed line: second-generation 3D mode $a_{10}b_{10}$. Dotted lines: third-generation 3D mode $a_{10,1}b_{10,1}$. Circles: bifurcation points. Triangles: states for which distributions of current density over the cathode surface are shown in (*b*). (*b*) Distributions of current density over the cathode surface for states belonging to the 3D modes shown in *a*). Bar in Am^{-2}.

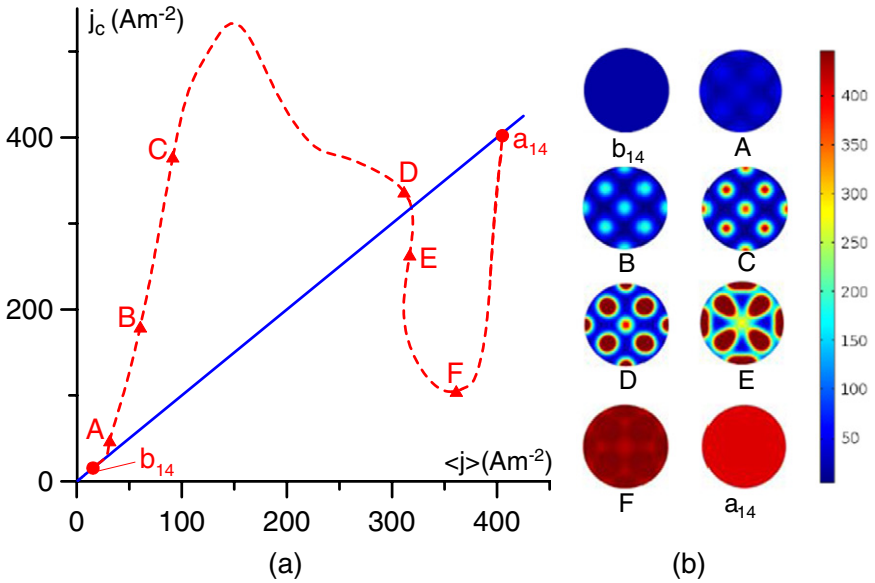

Figure 3. (*a*) Bifurcation diagram of the 14th multidimensional mode in krypton, $R = h = 0.5$ mm. Solid line: 1D mode. Dashed line: second-generation 3D mode $a_{14}b_{14}$. Circles: bifurcation points. Triangles: states for which distributions of current density over the cathode surface are shown in (*b*). (*b*) Distributions of current density over the cathode surface for states belonging to the 3D mode shown in (*a*). Bar in Am^{-2}.

to the point of minimum. As pressure is decreased, the falling section gradually disappears and the bifurcation points shift in the direction towards each other. At a pressure of 30Torr for xenon and 58 Torr for krypton and for lower pressures, the falling section is absent, as well as the bifurcation points.

When the bifurcation points disappear, so do multiple solutions, although eventually with a small delay, see figure 4 of [10]. Thus, there is a minimum pressure for each gas (and each discharge geometry) below which multiple solutions and therefore the self-organization do not exist; this pressure is the one at which the falling section of the CDVC disappears, or, as is sometimes said, the discharge becomes obstructed; for krypton microdischarges this pressure is roughly twice the one for xenon.

Several multidimensional modes for krypton have been computed. The current–voltage characteristics (CVCs) of the 3D modes with many spots in some ranges of discharge current almost coincide with the CVC of the 1D mode. Such modes are more conveniently represented in the coordinates $(\langle j \rangle, j_c)$, where $\langle j \rangle$ is the average value of the axial component of the electric current density evaluated over the discharge cross section and j_c is the current density at the centre of the cathode. As an example, three 3D modes are shown in figures 2 and 3. $a_{10}b_{10}$ and $a_{14}b_{14}$ represent the 10th and 14th multidimensional modes which bifurcate from and rejoin the 1D solution; the so-called second-generation modes. $a_{10,1}d_{10,1}$ represents a third-generation mode which bifurcates from the mode $a_{10}b_{10}$.

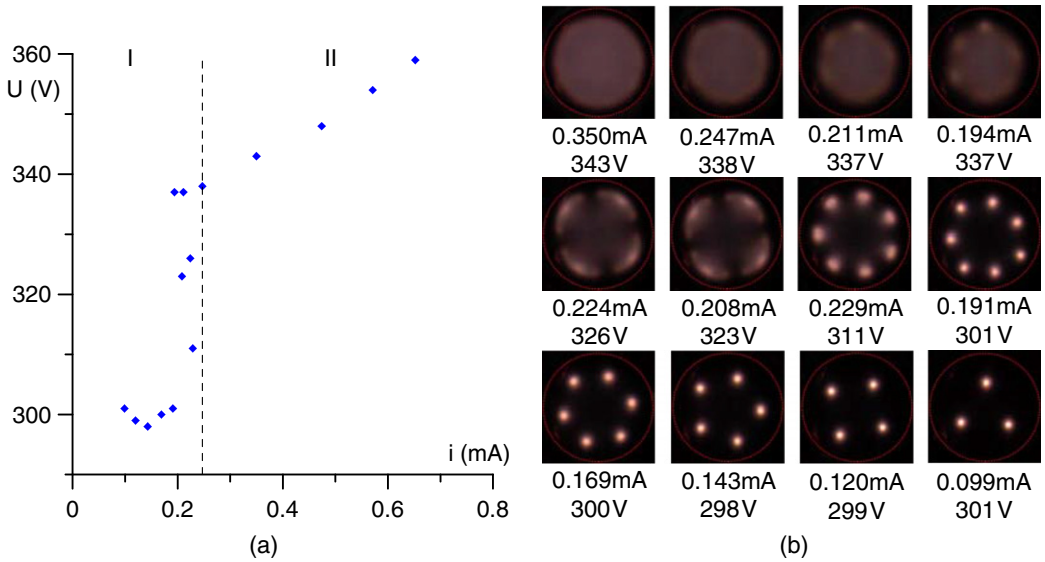

Figure 4. Krypton, 150 Torr; $h = 250\,\mu$m, $R = 375\,\mu$m. (*a*) Experimentally measured CVC. Region I: range of discharge currents where self-organization is present. Region II: abnormal (diffuse) discharge. (*b*) End-on images of the discharge plasma corresponding to states represented in figure 4(*a*).

The modes $a_{10}b_{10}$ and $a_{14}b_{14}$ have been previously computed in xenon for 30 Torr (the modes designated $c_8 f_8$ and $c_{12} f_{12}$, respectively, of [11]), argon for 75 Torr and in helium for 530 Torr (the modes designated $c_8 f_8$ and $c_{12} f_{12}$, respectively, of [14]). The mode $a_{10}b_{10}$ is considerably richer in spot patterns and hysteresis phenomena in krypton than in xenon, argon and helium. The spot pattern associated with the mode $a_{14}b_{14}$ is similar to the corresponding mode computed in helium, the main difference being a larger size of the spots for a certain range of discharge currents, see states *D* and *E*. The mode $a_{10,1}b_{10,1}$ is similar to the corresponding mode computed for helium for 530 Torr (the mode $d_1 g_1$ of [14]). Note that a discussion of the above-mentioned modes in a general context of the theory of self-organization in bistable nonlinear dissipative systems can be found in [16].

3. Experiment

The CBLD device used in this study is comprised of a planar Mo cathode and a perforated Mo anode. The two electrodes are separated by a quartz disc with the same size concentric opening as on the anode. Each layer is approximately 250 μm thick and the openings on the quartz disc and the anode are of 750 μm in diameter. The cathode is polished with 400 grit, 800 grit and 1200 grit SiC sandpaper on a polishing machine. The final step was carried out with a polishing cloth with 3 μm polycrystalline diamond paste to achieve a mirror-like cathode surface condition. The three layers are assembled via Torr Seal® and annealed in a box oven at 120 °C for half an hour. The fully assembled device is then held in a vacuum chamber which is pumped down to a base pressure of ~0.4 mTorr. Research grade krypton (99.999%) is introduced into the chamber to desired pressure and kept static till the next pump down and refill cycle.

A copper wire is used to connect the cathode disc to an electrical feedthrough on the chamber, which is further connected to a current limiting dc negative polarity power supply (Glassman®) via a ballast resistor (100 kΩ) and a current monitoring resistor (1 kΩ). An over voltage (current limited to approximately 1 mA) is provided for the initial ignition of the device. Current is then gradually reduced till the plasma extinguished. Two high voltage potentiometers (0–200 kΩ) are also connected in series in the circuit for fine tuning of discharge current; it is worth stressing that the distinguishing feature of the present setup from previous work [1–4, 6] is the inclusion of these high voltage potentiometers. Discharge voltage is taken via a multimeter that can measure up to 1500 V dc. Discharge current is converted from the voltage measured across the current monitoring resistor.

A Panasonic GP-KR222 charge coupled device (CCD) camera together with a telescope lens is used to record visible spectrum video of the discharges through a quartz viewport on the vacuum chamber. Snapshots of the discharges are digitally recorded via a Hauppauge video box. A schematic of the experimental setup is the same as shown in figure 1 of [15].

A few exemplary end-on visible-spectrum photographs of discharge operated in krypton at pressures from 150 to 301 Torr are shown in figure 4. No self-organization was observed in krypton at 60 Torr. At pressures above 120 Torr, clustered light emission was observed (see figure 5). These clusters became confined to smaller areas at higher pressures with higher overall discharge currents. These results are in good correspondence with the trend predicted by the modelling: the above-mentioned minimum pressure of 120 Torr is about two times higher than what is required for formation of self-organized patterns in xenon in this particular device, which is roughly 50 Torr. It is interesting to note, however, that after obtaining the minimum number of spots at the self-organization onset pressure, lowering gas pressure in the vacuum chamber may reduce the number of spots until the extreme case of a single spot at the centre of the opening. Depending on the sample condition, this action may also lead to the extinction of the plasma immediately.

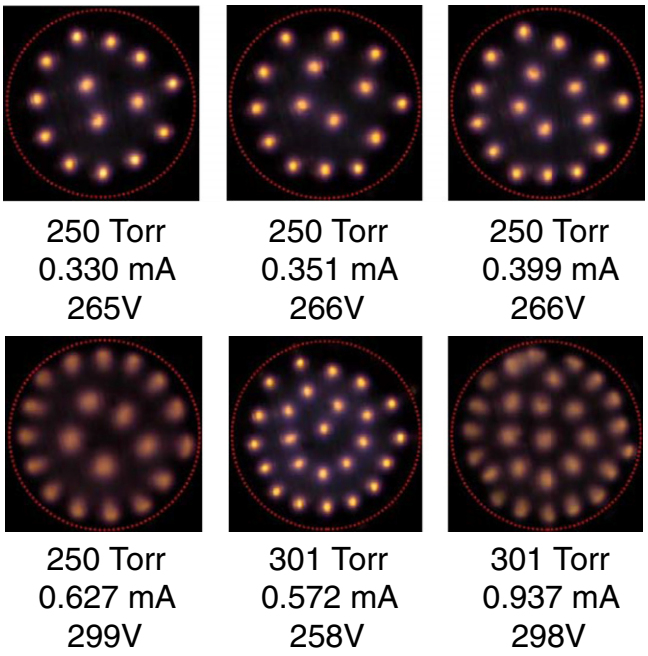

Figure 5. Experimentally observed self-organized spot patterns in krypton for different pressures, $h = 250\,\mu$m, $R = 375\,\mu$m.

The measured CVC at 150 Torr is shown in figure 4. Similarly to the case of xenon [1], this CVC can be divided into two regions. In region *I* in the figure, the self-organized patterns of spots are observed. Region *II* corresponds to the abnormal discharge. Examples of the patterns observed in region *I* are shown in figure 4(*b*), as well as a few images corresponding to states in the abnormal discharge where a homogeneous plasma covers the surface of the cathode. The patterns shown in figure 4(*b*) (and observed in krypton for 150 Torr) are similar to those observed in xenon for 75 Torr, see figure 4 of [1] and figure 3 of [2].

It should be stressed that an over current (or full ignition of the device) is necessary at the beginning: stable patterns in region *I* of the CVC can only be obtained by lowering the discharge current to that range from region *II*. Within region *I*, however, carefully raising and lowering current may lead to different patterns without having to go through region *II* of the CVC. It also appears that hysteresis within region *I* exists and it will be reported separately elsewhere.

Pattern formation is accompanied by a sharp decrease in the discharge voltage when the current is reduced, as evidenced in figure 4(*a*). When current is reduced, the plasma starts to contract towards the centre of the circular opening (i.e., stripping away from the periphery of the opening), covering less and less cathode surface. First sign of the pattern formation is represented by big clumps of plasma separated from each other and regularly arranged, followed by the formation of more well-defined spots. Lowering the current further reduces the size of each spot to roughly 70 μm while maintaining the number of spots the same. Further reduction of the current reduces the number of filaments until the lowest number of spots has been reached, after which the plasma completely extinguishes. Each well-defined spot carries approximately 0.03 mA, which can be easily verified from pictures in figure 4. With an increase of pressure, the region *I* of the CVC shifts to higher values of the discharge current. All these features are similar to what have been observed in xenon [1].

It should be noted that self-organization in krypton seems to be much more sensitive to the surface condition of the cathode than in xenon. Despite the cathode being carefully prepared and cleaned, self-organization in krypton for some samples is not observed consistently at the initial stage of the experiment when current is slowly lowered: at higher currents, plasma occupies the entire cathode surface within the cavity; when current is lowered, plasma first becomes weaker throughout the cavity and then on some occasions starts to shrink, covering only part of the cathode until it completely diminishes, i.e., the normal discharge occurs. Conditioning of the cathode surface is helpful for such samples: the samples are operated in xenon first at approximately 100 Torr for about half an hour. At this stage, self-organization in xenon is easily achieved. The vacuum chamber is then pumped down to ~0.4 mTorr and refilled with krypton to 150 Torr. Only then, we were able to obtain self-organization easily. We suspect that during this 'conditioning period' in xenon, thin layers of surface oxide formed during the annealing process of the sample preparation are removed by ion bombardment, thus affecting the secondary electron emission.

4. Conclusions

It is shown experimentally that, in agreement with the theoretical predictions, self-organization in dc glow microdischarges is not particular of xenon: self-organized patterns have been observed in microdischarges in krypton. The pressure required for the onset of self-organization in krypton is roughly twice that pressure in xenon, again as predicted by the theory.

As predicted by the theory, the experimentally observed self-organized spot patterns in krypton are similar to the ones observed in xenon [1–7]. On the other hand, condition of the cathode surface has a bigger effect on self-organization in krypton than in xenon. It has also been found that the erosion of the cathode surface in krypton is faster than in xenon.

This work and the modelling of the preceding works [12–14] concern the effect produced over self-organization by the species of plasma-producing gas. A related question is what is the effect of cathode material and condition of the cathode surface. Some experimental indications are available; for example, it is known that some cathode materials (e.g., molybdenum, titanium, tungsten) are favourable for formation of self-organized patterns, some are rather hard to generate self-organization, and some (e.g., aluminum, stainless steel) do not generate self-organization at all. This effect deserves a systematic investigation via both experiment and modelling. Note that in the modelling this effect can be investigated by varying the secondary electron emission coefficient.

Acknowledgments

The authors are thankful to Dr Maria José Faria for providing the code which was used to perform bifurcation analysis.

The work at UMa was supported by FCT of Portugal through projects PTDC/FIS-PLA/2708/2012 *Modelling, understanding, and controlling self-organization phenomena in plasma-electrode interaction in gas discharges: from first principles to applications* and PEst-OE/MAT/UI0219/2014. D F N Santos is thankful to FCT of Portugal for support through the PhD grant SFRH/BD/85068/2012.

References

[1] Schoenbach K H, Moselhy M and Shi W 2004 *Plasma Sources Sci. Technol.* **13** 177–85
[2] Moselhy M and Schoenbach K H 2004 *J. Appl. Phys.* **95** 1642–9
[3] Takano N and Schoenbach K H 2006 *Plasma Sources Sci. Technol.* **15** S109–S117
[4] Takano N and Schoenbach K H 2006 Self-organized patterns in cathode boundary layer discharges *Abstracts of the 2006 IEEE International Conf. on Plasma Science (Traverse City, MI)* IEEE p 247
[5] Lee B J, Rahaman H, Frank K, Mares L and Biborosch D L 2007 Properties of the MHCD in xenon *Proc. 28th ICPIG (Prague, Czech Republic, July 2007)* ed J Schmidt *et al* (Prague: Institute of Plasma Physics AS CR) ISBN 978-80-87026-01-4 pp 900–2
[6] Zhu W, Takano N, Schoenbach K H, Guru D, McLaren J, Heberlein J, May R and Cooper'J R 2007 *J. Phys. D: Appl. Phys.* **40** 3896–906
[7] Lee B J, Biborosch D L, Frank K and Mares L 2008 *J. Optoelectron. Adv. Mater.* **10** 1972–5
[8] Moselhy M, Petzenhauser I, Frank K and Schoenbach K H 2003 *J. Phys. D: Appl. Phys.* **36** 2922
[9] Almeida P G C, Benilov M S, Cunha M D and Faria M J 2009 *J. Phys. D: Appl. Phys.* **42** 194010
[10] Almeida P G C, Benilov M S and Faria M J 2010 *Plasma Sources Sci. Technol.* **19** 025019
[11] Almeida P G C, Benilov M S and Faria M J 2011 *IEEE Trans. Plasma Sci.* **39** 2190–1
[12] Almeida P G C, Benilov M S and Faria M J 2011 Predicting formation of self-organized patterns of cathodic spots in dc glow microdischarges in argon and helium *Proc. 30th Int. Conf. on Phenomena in Ionized Gases (Belfast, UK, 28 August–2 September 2011)* http://mpserver.pst.qub.ac.uk/sites/icpig2011/437_A4_Almeida.pdf
[13] Almeida P G C and Benilov M S 2012 Self-organization as an intrinsic feature of dc glow microdischarges: modelling appearance of different spot patterns *Proc. ESCAMPIG 2012 (Viana de Castelo, Portugal, 10–14 July 2012)* ed P G C Almeida *et al* (ISBN 2-914771-74-6) http://escampig2012.ist.utl.pt/Proceedings
[14] Almeida P G C and Benilov M S 2013 *Phys. Plasmas* **20** 101613
[15] Zhu W and Niraula P 2014 The missing modes of self-organization in cathode boundary layer discharge in xenon *Plasma Sources Sci. Technol.* **23** 054011
[16] Benilov M S 2014 Multiple solutions in the theory of dc glow discharges and cathodic part of arc discharges. Application of these solutions to the modeling of cathode spots and patterns: a review *Plasma Sources Sci. Technol.* **23** 054019
[17] Almeida P G C, Benilov M S and Santos D F N 2014 Modelling self-organization in DC glow microdischarges: new 3D modes arXiv:1406.4394A
[18] Biondi M A and Chanin L M 1954 *Phys. Rev.* **94** 910–6
[19] Raizer Yu P 1991 *Gas Discharge Physics* (Berlin: Springer)
[20] Hagelaar G J M and Pitchford L C 2005 *Plasma Sources Sci. Technol.* **14** 722–33
[21] Lukác P, Mikuš O, Morva I, Zábudlá Z, Trnovec J, Morvová M and Hensel K 2012 *Plasma Sources Sci. Technol.* **21** 065002